J Neurophysiol 89: 324–337, 2003;
10.1152/jn.00729.2002.

Persistent Na^+ Current Modifies Burst Discharge By Regulating Conditional Backpropagation of Dendritic Spikes

BRENT DOIRON,[1] LIZA NOONAN,[2] NEAL LEMON,[2] AND RAY W. TURNER[2]
[1]*Department of Physics, University of Ottawa, Ottawa, Ontario K1N 6N5;* [2]*Neuroscience Research Group, Department of Cell Biology and Anatomy, University of Calgary, Calgary, Alberta, T2N 4N1 Canada*

Submitted 26 August 2002; accepted in final form 20 September 2002

Doiron, Brent, Liza Noonan, Neal Lemon, and Ray W. Turner. Persistent Na^+ current modifies burst discharge by regulating conditional backpropagation of dendritic spikes. *J Neurophysiol* 89: 324–337, 2003; 10.1152/jn.00729.2002. The estimation and detection of stimuli by sensory neurons is affected by factors that govern a transition from tonic to burst mode and the frequency chracteristics of burst output. Pyramidal cells in the electrosensory lobe of weakly electric fish generate spike bursts for the purpose of stimulus detection. Spike bursts are generated during repetitive discharge when a frequency-dependent broadening of dendritic spikes increases current flow from dendrite to soma to potentiate a somatic depolarizing afterpotential (DAP). The DAP eventually triggers a somatic spike doublet with an interspike interval that falls inside the dendritic refractory period, blocking spike backpropagiation and the DAP. Repetition of this process gives rise to a rhythmic dendritic spike failure, termed conditional backpropagation, that converts cell output from tonic to burst discharge. Through *in vitro* recordings and compartmental modeling we show that burst frequency is regulated by the rate of DAP potentiation during a burst, which determines the *time* required to discharge the spike doublet that blocks backpropagation. DAP potentiation is maginfied through a postitve feedback process when an increase in dendritic spike duration activates persistent sodium current (I_{NaP}). I_{NaP} further promotes a slow depolarization that induces a shift from tonic to burst discharge over time. The results are consistent with a dynamical systems analysis that shows that the threshold separating tonic and burst discharge can be represented as a saddle-node bifurcation. The interaction between dendritic K^+ current and I_{NaP} provides a physiological explanation for a variable time scale of bursting dynamics characteristic of such a bifurcation.

INTRODUCTION

The output pattern of central neurons in response to membrane depolarization is a crucial element of signal processing. Two important aspects of spike output with respect to sensory processing are the ability to shift from tonic to burst mode and the regulation of burst frequency. A switch from tonic to burst mode has been proposed to reflect a shift from stimulus estimation to stimulus detection (Sherman 2001), an hypothesis that has experimental support in the electrosensory system (Bastian et al. 2002; Gabbiani et al. 1996). The regulation of burst frequency can influence the ability of neurons to contribute to different behavioral states (Steriade et al. 1990) and in the synchronization of networks (Lisman 1997). Cells discharging spike bursts in the γ-frequency range (40 to >80 Hz) have been reported from the cortical to spinal levels, indicating a role for this output in signal processing at all levels of the CNS (Gray and McCormick 1996; Steriade et al. 1993, 1998; Turner et al. 1994).

Gamma-frequency bursts in pyramidal cells of the electrosensory lateral line lobe (ELL) of weakly electric fish rely on a "conditional backpropagation" of Na^+ spikes from somatic to dendritic membranes (Doiron et al. 2001, 2002; Lemon and Turner 2000). This mechanism arises when spikes backpropagating from the soma fail in their active conduction $\sim$200 μm from the soma. Spikes thus rapidly increase in duration from $\leq$1 ms at the soma to $\geq$10 ms as they approach their point of failure in the proximal dendrites. This basic difference in somatic and dendritic spike durations allows current flow associated with dendritic spike discharge to reexcite the soma as a depolarizing afterpotential (DAP). During repetitive discharge, a frequency-dependent broadening of dendritic spikes potentiates the DAP to the point of triggering a somatic spike doublet. The short interspike interval of the doublet falls inside the dendritic refractory period with the result that the second spike of the pair fails to backpropagate. The resulting loss of dendritic depolarization and somatic DAP then allows the cell to repolarize and generate an interburst interval. By repeating this process, pyramidal cells generate a rhythmic series of spike bursts that extend into the γ-frequency range.

The ability for conditional backpropagation to underlie burst discharge reveals that the *failure* of spike backpropagation from soma to dendrite can exert a direct control over cell output. Compartmental modeling has indicated that conditional backpropagation can be induced at least through a cumulative inactivation of dendritic K^+ current (Doiron et al. 2001). The present study used experimental analysis and modeling to further examine the somatic and dendritic mechanisms that regulate conditional backpropagation and burst discharge. We show that burst frequency is directly related to the rate of DAP potentiation at the soma, which establishes the time required to generate a spike doublet. The rate of DAP potentiation can be accounted for by a positive feedback process between a cumulative inactivation of dendritic K^+ current and persistent sodium current (I_{NaP}) that amplifies depolarizations underlying conditional backpropagation. A slow activation of I_{NaP} further induces a transition from tonic to burst discharge over time. Finally, our results are consistent with a dynamical systems analysis, which predicted that a saddle-node bifurcation separates tonic and burst discharge in pyramidal cells (Doiron et al.

Address for reprint requests: R. W. Turner, Neuroscience Research Group, University of Calgary, 3330 Hospital Dr. N.W., Calgary, Alberta, Canada T2N 4N1, (E-mail: rwturner@ucalgary.ca).

2002). The present work thus identifies the ionic factors that control the rate of passage through a trapping region (ghost) of the saddle-node bifurcation, illustrating an efficient mechanism to control the frequency of burst discharge.

METHODS

Apteronotus leptorhynchus (Brown Ghost Knife fish) were obtained from local importers and maintained at 26–28°C in fresh water aquaria. Anesthesia prior to dissection was obtained using 0.05% phenoxy-ethanol applied in the tank water and during gill perfusion as accepted by the Canadian Council of Animal Care. The procedures for preparing and maintaining ELL tissue slices have been previously described (Lemon and Turner 2000; Turner et al. 1994). All chemicals were obtained from Sigma (St. Louis, MO) unless otherwise noted. Slices were cut along the transverse or longitudinal axis of the ELL and maintained at room temperature as an interface preparation using artificial cerebrospinal fluid (ACSF) containing (in mM) 124 NaCl, 2.0 KCl, 1.25 KH_2PO_4, 1.5 $CaCl_2$, 1.5 $MgSO_4$, 24 $NaHCO_3$, and 10 D-glucose, pH 7.4. Drugs were focally ejected as described previously (Turner et al. 1994).

Intracellular recordings were obtained from pyramidal cell bodies within the pyramidal cell layer ($n = 64$) and from apical dendrites within 200 μm of the cell body layer ($n = 42$) in the centromedial segment (CMS) of the ELL. Glass microelectrodes were backfilled with 2 M KAc (pH 7.4; ~90 MΩ resistance). In a random selection of recordings, the input resistance at the soma was 64 ± 21.9 (SD) MΩ ($n = 24$) and in apical dendrites 59 ± 19.7 MΩ ($n = 20$). Direct current injection of −0.1 to −0.5 nA was applied when necessary to eliminate spontaneous discharge. Antidromic spikes were evoked by placing a concentric bipolar electrode on pyramidal cell axons in the plexiform layer that courses beneath the pyramidal cell layer. Recordings were digitized (CED, Cambridge, UK) and stored for off-line analysis (Igor Pro, Wavemetrics, Lake Oswega, OR; Corel Draw, Ottawa, ON, Canada). All average values are expressed as means ± SD. Data plots were constructed and regression analyses performed using Microcal Origin (Northampton, MA).

Burst detection

In the majority of recordings, the occurrence and characteristics of burst discharge were extracted using custom software (Igor Pro). We have previously detected spike bursts generated during a slower form of oscillation in pyramidal cells by using interspike interval (ISI) histograms to define a threshold that demarked burst and intraburst ISIs (Turner et al. 1996). However, a shift in ISIs over time during long depolarizations (Fig. 7*A*) indicates a nonstationarity in the relevant data set that prevents this form of statistical analysis (Gabbiani and Koch 1998). A second approach to identify bursts was to define a minimal sequence of decreasing ISIs in the spike train. This would appear to be highly applicable to the burst discharge studied here given the clear decrease in ISIs that lead up to spike doublet generation at lower intensities of stimulation (Lemon and Turner 2000). However, we found that this method was not effective, as pyramidal cell bursts are composed of only a repeating series of spike doublets at higher intensities (Lemon and Turner 2000; Turner et al. 1994). We were able to define burst discharge using the difference of consecutive ISIs (Holt et al. 1996), although with an unacceptable level of error. Rather, we found that the large burst afterhyperpolarization (AHP) that consistently follows a spike doublet (Lemon and Turner 2000) was the most reliable indicator of the occurrence of burst discharge (Fig. 1, *A* and *B*).

We thus used the difference between consecutive AHP amplitudes to detect the occurrence of conditional backpropagation and from this the nature of events during spike bursts. Specifically, we calculated the local difference σ_i between consecutive AHPs $i - 1$ and i as $\sigma_i = (\mathrm{AHP}_i - \mathrm{AHP}_{i-1})^2$. AHP amplitudes were computed as the trough between two action potentials, and the difference was squared to increase the sensitivity of our measure. Given a spike train of N spikes, this gave a sequence of $N - 1$ σ values. The σ measured between the AHP within a spike doublet, and the following burst AHP was much larger than the σ measured between other AHPs. We set a threshold value, σ_{thres}, and marked the ith AHP as a burst AHP if σ_{i-1} and σ_i satisfied the conditions $\sigma_{i-1} < \sigma_i$ and $\sigma_i > \sigma_{\mathrm{thres}}$ (Fig. 1). The accuracy of burst detection was finally cross-checked by visually inspecting data records to verify that the detection threshold was adequate to define burst AHP occurrence. The ability to use burst AHPs to identify a change in firing mode was indicated by the transition of ISI histogram plots from one of a monophasic to biphasic structure after the onset of burst AHPs (see Fig. 2*C*). However, the nonstationarity of the data over long depolarizations (see Fig. 7*A*) allows only qualitative results to be inferred from these histograms, requiring that we use the occurrence of burst AHPs

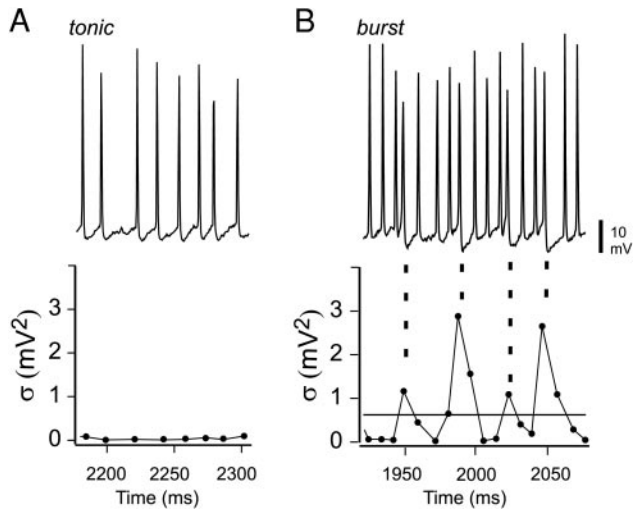

FIG. 1. Method of analysis for identifying the occurrence of burst discharge. *A* and *B*: afterhyperpolarization (AHP) amplitude is calculated as the minimum absolute voltage within an interspike interval. The difference between the squares of consecutive AHP amplitudes (σ) distinguishes *tonic* (*A*) from *burst* discharge (*B*) during a long depolarizing current pulse (4 s) in a somatic recording. *A*: tonic spike discharge is associated with little change in AHP amplitudes over time with a correspondingly low σ between consecutive interspike intervals (ISIs, *bottom*). *B*: during burst discharge, the comparatively large amplitude of burst AHPs is associated with a sharp transition in the σ measured from the AHP within the doublet and the subsequent burst AHP (- - -, the correspondence between σ and the burst AHP). The σ threshold (σ_{thres}) used to time stamp the occurrence of burst AHPs is shown by ——— in *B*, a value cross-checked in each case against actual data records to verify the accuracy of threshold determination. Burst AHPs were used as reference points to identify the occurrence of individual bursts to subsequently extract several parameters for analysis.

to demark points for burst analysis. This method proved to be less effective for cases in which burst AHP amplitude approached that of intraburst AHPs, such as found in some dendritic recordings. For this reason, automated burst analysis was restricted to somatic recordings. In a limited number of cases, analysis of burst properties were conducted manually to ensure accuracy if burst AHP amplitudes were not sufficiently large for automated analysis.

In all experiments, the resting potential of the cell was adjusted through slight current injection to remove all spontaneous discharge. When depolarizing current is injected under these conditions, the ISIs progressively decrease toward the generation of a spike doublet and burst AHP (Lemon and Turner 2000). Therefore, all ISIs occurring between consecutive burst AHPs were assumed to represent intraburst intervals. In some cases, burst discharge was temporarily interrupted by a cessation of spike activity after ~2 s of depolarization. Burst analysis in these cells was restricted to only the initial portion of the record.

We estimated the rate of DAP potentiation (defined as Δ; Fig. 2*A*) as the slope of the net change in potential from the trough of the first AHP (absolute negative peak) to the deflection point of the second spike of the spike doublet. Although this will overestimate the absolute voltage shift associated with DAP potentiation, this approach is validated by our previous work showing that all depolarizing shifts within a burst can be attributed to changes in only the DAP and not AHPs (Lemon and Turner 2000). Because the inflection indicating a DAP could be difficult to detect on the first spike of a burst, we chose to use the more reliable measure of the trough of the first AHP. Control experiments measuring only the deflection of the DAP during a burst for the clearest cases produced comparable results, including all correlations between DAP amplitude and oscillatory discharge. Our stated values of DAP potentiation are thus estimates that were used to compare the relative rate of change under different conditions.

Compartmental modeling

We previously developed a compartmental model of an ELL pyramidal cell using the simulation software NEURON (Hines and Carnevale 1997). The compartmentalization (300+ com-

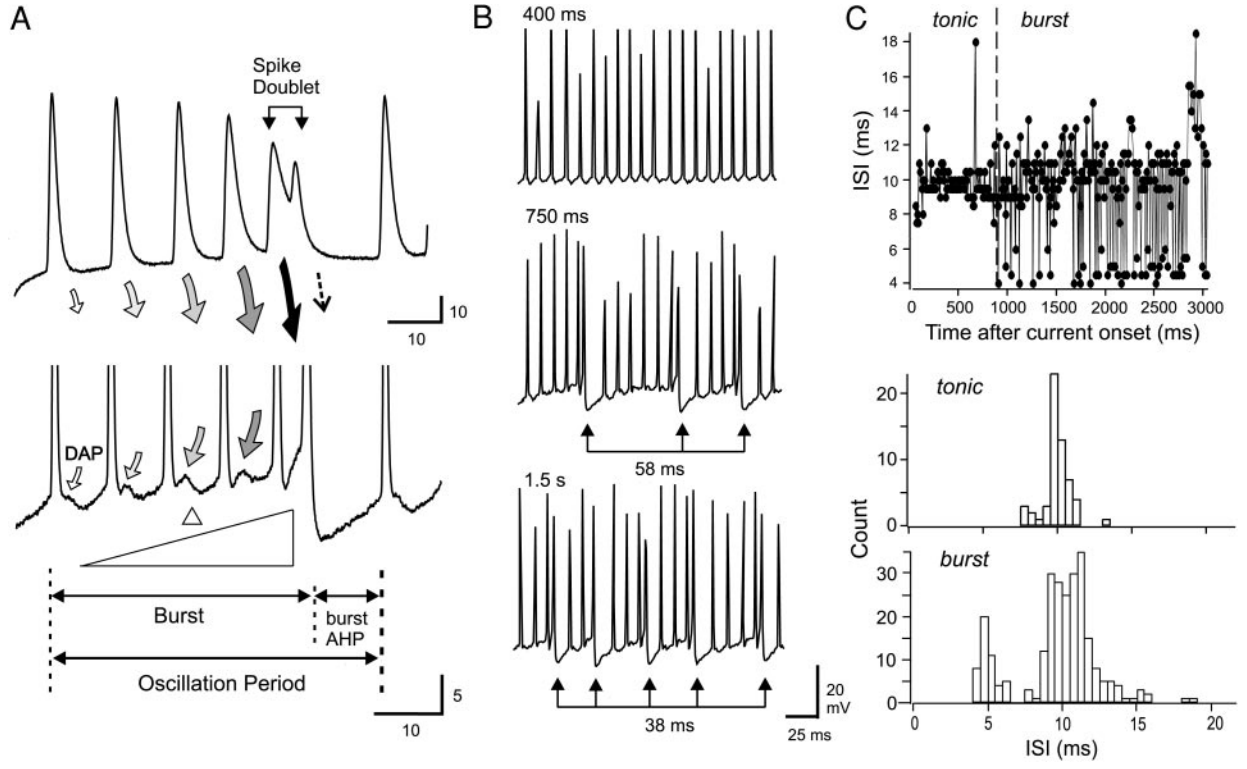

FIG. 2. Oscillatory spike bursts are triggered through conditional spike backpropagation. *A*: summary diagram of the factors underlying conditional spike backpropagation and burst discharge (Lemon and Turner 2000). Somatic and dendritic recordings from separate pyramidal cells are aligned to construct a schematic of interactions during repetitive discharge. Each spike initiated at the soma backpropagates over the initial 200 μm of dendrites, leading to a broad dendritic spike that promotes return current flow to re-excite the soma as a DAP (arrows). A frequency-dependent broadening of dendritic spikes increases dendrosomatic current flow until generating a somatic spike doublet that exceeds the dendritic refractory period and blocks backpropagation. A subsequent burst AHP is recorded at the somatic and dendritic level. One oscillation period is defined as the combined duration of a spike burst and subsequent burst AHP, and the rate of DAP potentiation as Δ. *B*: spike discharge shifts from tonic to burst output 750 ms after the onset of a 4 s depolarizing current pulse (0.74 nA) initially set subthreshold for burst discharge (*top*). Arrows denote the occurrence of burst AHPs. The time for each recording is shown on the top left and mean oscillation period below. The variation in spike height results from a low sampling rate. *C*: a plot of ISI over time for the cell shown in *B* indicates a dramatic increase in the variability upon the occurrence of burst discharge (*top*), with the rhythmic downward deflections indicating burst AHP ISIs. ISI histograms calculated below for the *tonic* and *burst* phase of spike discharge reveal a clear shift to a bimodal ISI distribution after the occurrence of burst discharge. Nonstationarity of the data set allows only for qualitative inferences from the histograms (unimodal vs. bimodal).

partments) was based on confocal images of a Lucifer-yellow-dye-filled ELL basilar pyramidal cell. The model dynamics were based on 10 ion channels with kinetic properties that were constrained by biophysical and electrophysiological data (Doiron et al. 2001). Of specific interest was the modeling of a persistent Na^+ current (I_{NaP}) that exists over the soma and proximal apical dendrites of pyramidal cells and provides a voltage- and TTX-sensitive boost of EPSPs (Berman et al. 2001). The parameters of I_{NaP} were chosen to reproduce this effect on excitatory postsynaptic potentials (EPSPs), requiring a τ_m of activation = 0.2 ms. The current study extends this description to model the time course of I_{NaP} activation in pyramidal cells, which has been shown to generate a depolarization that can last for hundreds of milliseconds following a short train of synaptic input (Berman et al. 2001). To simulate this slow depolarization, we replaced our original treatment of I_{NaP} with $I_{NaP,S}$, which uses both the original and a slower time scale of activation; $I_{NaP,S}$ was described as

$$I_{NaP,S} = g_{max,NaP,S} \cdot m \cdot s \cdot (V_m - E_{Na}) \quad (1)$$

$$s_\infty(V_m) = (1 + e^{-(V_m - V_{1/2,s})/k_s})^{-1} \quad (2)$$

$$\frac{ds}{dt} = \frac{s_\infty(V_m) - s}{\tau_s} \quad (3)$$

Equation 1 gives the I_{NaP} in which $g_{max,NaP,S}$ represents the NaP channel density (10 mS/cm^2 in the somatic compartment and 3 mS/cm^2 in the 1st 10 proximal apical dendritic compartments), E_{Na} is the reversal potential for Na^+ (40 mV), and m (fast activation) and s (slow activation) are the dynamical gating variables controlling NaP activation. The kinetics and dynamics of m are described in Doiron et al. (2001). The steady-state kinetics of s is given by *Eq. 2* where $V_{1/2,s}$ (−58.5 mV) and k_s (6 mV) were set so that NaP activation is low threshold; these parameters are identical to the steady state of m [$m_\infty(V_m) = s_\infty(V_m)$]. The dynamics of s are given in *Eq. 3* with the time constant of activation, τ_s, set to 1.5 s, as determined by fitting the slope of the linear rise of a slow membrane potential shift in pyramidal cells during 4-s current pulses (2.9 mV/s; see Figs. 6*E* and 7*A*). $g_{max,NaP,S}$ was set larger than $g_{max,NaP}$ so as to compensate for the new state variable s, yet ensured that the net NaP and NaP,S steady-state currents were nearly equivalent. All model simulations in the current project used the NaP kinetics described in Doiron et al. (2001) until we extend our treatment of NaP to model the slow depolarization described by NAP,S (Figs. 7 and 8).

RESULTS

Conditional backpropagation and burst discharge

Current-evoked depolarizations trigger burst discharge that can be recorded in pyramidal cell somata and apical dendrites (Lemon and Turner 2000). Individual spike bursts are comprised of two to seven spikes with a progressively decreasing ISI that culminates in the generation of a spike doublet and subsequent burst AHP. The burst AHP is largest at the soma and effectively inhibits spike discharge for up to 40 ms, providing a pause between spike bursts. The same pattern of spike burst and burst AHP is recorded at the somatic and dendritic level, although with differences in spike and AHP amplitudes.

The process of conditional backpropagation is summarized in the schematic diagram of Fig. 2*A*. Pyramidal cells initiate spike discharge at the somatic level, followed by an active Na^+ spike backpropagation over the initial 200 μm of a 500 to 800 μm dendritic tree. The proximal dendritic spike broadens quickly with respect to the somatic spike, leading to return current flow that generates a DAP at the soma. We have shown that spikes in dendritic membrane exhibit a frequency-dependent broadening during repetitive discharge at ISIs of 3–14 ms (Lemon and Turner 2000). Return current flow to the soma is thus increased during repetitive discharge, potentiating the DAP to the point of triggering a somatic spike doublet. The spike doublet is critical to burst discharge as the short ISI separating the spike pair falls within the dendritic refractory period, abruptly terminating the dendritic depolarization that generates the DAP. The sudden loss of dendritic depolarization from one spike to the next allows a burst AHP to repolarize the cell. Repetition of this process gives rise to oscillatory burst discharge in the γ-frequency range. A recently constructed compartmental model supported this hypothesis by revealing that a cumulative inactivation of dendritic K^+ current can induce the process of conditional backpropagation through dendritic spike broadening (Doiron et al. 2001). The physiological importance of this mechanism was recently established by the recording of conditional backpropagation at the dendritic level of pyramidal cells during sensory processing in vivo (J. Bastian, personal communication).

Lemon and Turner (2000) reported that oscillatory burst discharge generated in this manner can span a range of at least 100 Hz; an exceptionally wide range of frequencies for a bursting neuron. In other cells a shift in burst frequency results from changes in the burst and/or interburst interval according to such factors as the number or frequency of spikes per burst, which can affect Ca^{2+} influx and a subsequent AHP (Golding et al. 1999; Tegner et al. 1998). However, we have determined that burst discharge in pyramidal cells of the centromedial segment of the ELL is not sensitive to either Cd^{2+} or Ni^{2+} ejections (Noonan and Turner, unpublished observations). This indicates that pyramidal cells rely on different mechanisms to control burst frequency.

A primary objective of this study was to identify the factors within the burst or interburst interval that control burst frequency in pyramidal cells. A second objective was to identify the mechanism by which pyramidal cells can switch from a tonic to burst discharge.

Pyramidal cell output

Pyramidal cells generate a relatively tonic pattern of spike output when depolarized to near spike threshold (Turner et al. 1994). However, over the duration of a 4 s current pulse, 80% of pyramidal cells shifted from a tonic to burst discharge, revealing a time-dependent change in the pattern of spike output (Fig. 2*B; n* = 16/20; 0.2–0.6 nA). The transition from a tonic to burst output was evident by the onset of spike doublets and burst AHPs (Fig. 2, *B* and *C*) that signified a switch from a monophasic to biphasic structure of ISI histograms (Fig. 2*C*). The biphasic ISI histogram during burst discharge represents an early peak of high-frequency spike doublets (4–6 ms) and a second peak of ISIs that lead up to spike doublet discharge (7–12 ms) that includes an elongated tail associated with burst AHPs (12–18 ms). At the initial onset

of burst discharge, oscillation period ranged between 63 and 186 ms (mean of 117 ± 43.5 ms; $n = 16$) but decreased by up to 40 ms (e.g., mean of 21 ± 9.7 ms for the cell shown in Fig. 2*B*). In the present study, we used this current-evoked decrease in oscillation period over time as a tool to identify the intra- or inter-burst factors that change in association with a shift in oscillation period.

Shifts in oscillation period are tightly linked to intraburst parameters

SPIKE BURSTS. We found that as oscillation period decreased during current injection there was a prominent and parallel decrease in burst duration (Fig. 3, *A* and *B*). There was a further decrease in the number of spikes per burst, eventually leading to a pattern of spike doublets and triplets as burst duration fell to a consistent value (Fig. 3*C*). In all cells examined, three factors were highly correlated with oscillation period ($n = 16$): burst duration ($r = 0.97 \pm 0.02$), the number of spikes per burst ($r = 0.96 \pm 0.03$), and the rate of DAP potentiation ($r = 0.89 \pm 0.07$; Fig. 3*D*), indicating that these burst properties are closely linked to oscillation period. A closer examination of the burst itself revealed that burst duration was also highly correlated to the number of spikes per burst ($r = 0.98 \pm 0.01$; $n = 16$) and the rate of DAP potentiation ($r = 0.91 \pm 0.06$; $n = 16$).

BURST AHP. Although a change in the duration of the burst AHP would provide the means to shift oscillation period, we found that neither the duration nor amplitude of the burst AHP changed over time (Fig. 3*B*; $n = 16$). This finding was supported in all cells by a lack of any correlation between the burst AHP and either oscillation period or burst duration, suggesting no clear link to ionic events during the burst (i.e. Ca^{2+} entry). Furthermore, burst AHP characteristics were not correlated with any aspect of the subsequent burst as would be predicted in cells controlling burst discharge through an interplay between the hyperpolarization-activated inward currents I_h and transient Ca^{2+} current (I_T) (Huguenard 1996; Pape 1996). Indeed, none of the factors we examined within spike bursts covaried with the burst AHP. We did find that burst AHP duration was reduced in a linear fashion as current intensity was increased ($n = 9$). However, at any given current level, both the amplitude and duration of the burst AHP were stable throughout the time course of depolarizations that shifted oscillation period. The burst AHP thus plays a role in allowing a recovery from intraburst events but not in the control of oscillation period during long depolarizations.

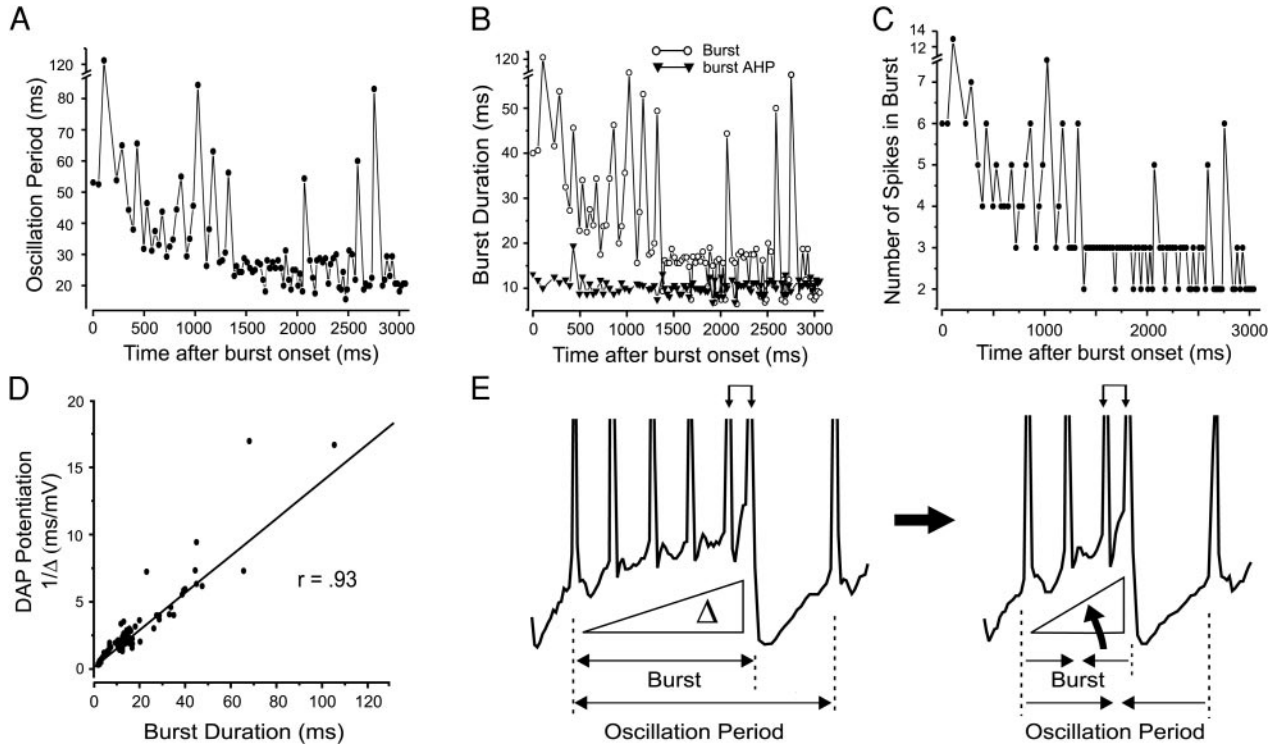

FIG. 3. A shift in oscillation period is associated with specific changes in intraburst properties. *A*: a plot of oscillation period after the onset of burst discharge (for cell shown in Fig. 2, *B* and *C*) reveals that oscillation period decreases from ~50–60 ms until stabilizing at ~20–30 ms. *B* and *C*: the duration of spike bursts (*B*) and the number of spikes per burst (*C*) decrease in concert with oscillation period over time. Note that burst AHP duration is stable as oscillation period is reduced (*B*). *D*: the rate of depolarizing afterpotential (DAP) potentiation during a burst is highly correlated to burst duration. *E*: hypothesis for the mechanism controlling oscillation period in pyramidal cells. Representative traces of single somatic bursts are shown to illustrate the factors that change as oscillation period decreases during long depolarizations. Double arrows above traces signify spike doublets, and spikes are truncated for illustrative purposes. A tonic depolarization reduces oscillation period from 57 ms at the onset of burst discharge (*left*) to 43 ms 3 s later (*right*). The DAP first increases at a rate $\Delta = 0.11$ mV/ms and at the higher rate of $\Delta = 0.16$ mV/ms at the end of the depolarization (large filled arrow). Note that an increase in the rate of depolarization allows the spike train to reach threshold for a spike doublet in a shorter period of time. As a result, the spike doublet reduces burst duration and the number of spikes per burst and thus oscillation period. In contrast, there is no significant change in burst AHP characteristics. Therefore shifts in oscillation period can be accounted for by the rate of DAP potentiation during a burst, which determines the *time* required to trigger the spike doublet that terminates spike backpropagation.

Control of oscillation period

Our results allow the formulation of an hypothesis of how conditional backpropagation can be modified to produce shifts in oscillation period (Fig. 3*E*). Because spike bursts are terminated by a spike doublet and burst AHP, burst duration should be highly dependent on the cell reaching threshold for the spike doublet. Therefore, the *time* required to reach threshold for the spike doublet is the critical determinant controlling burst duration and oscillation period. Importantly, the time to reach threshold for a spike doublet depends on the rate of DAP potentiation during repetitive discharge (Fig. 3*E*). A shortening of burst duration by the spike doublet also accounts for the number of spikes per burst, as reaching threshold for a spike doublet sooner will decrease the number of spikes discharged. The subsequent burst AHP reliably follows the spike doublet but is essentially uncoupled from other burst factors. The burst AHP is, nevertheless, critical for burst discharge in providing the interburst interval necessary to allow recovery of parameters that change during a burst.

Factors underlying potentiation of the DAP

The working hypothesis presented in the preceding text indicates that burst frequency depends in large part on the factors that control DAP amplitude. Lemon and Turner (2000) already established that changes in the DAP during repetitive discharge do not involve a shift in E_K, the properties of AHPs, or recurrent synaptic inputs. Rather, potentiation of the DAP occurs at ISIs of ~3–14 ms, which closely matches a frequency-dependent broadening of dendritic spikes. By using repetitive antidromic stimulation to induce burst discharge, we identified an ionic contribution in that both the dendritic spike and DAP could be boosted by membrane depolarization (Fig. 4). At the dendritic level, antidromic stimulus trains delivered between 3 and 10 ms ISI steadily increased the duration of dendritic spikes and the amplitude of an underlying depolarization that was produced as dendritic spikes summated (Fig. 4*A; n* = 7). Membrane depolarizations of 5–10 mV from rest further increased the rate of dendritic spike broadening and temporal summation during a stimulus train (Fig. 4, *A* and *B*). At the somatic level, antidromic stimulus trains at ISIs less than ~12 ms steadily potentiated the DAP (Fig. 4, *A* and *B; n* = 12). Membrane potential shifts at the soma were more complex in affecting both the DAP and AHPs, such that membrane hyperpolarization increased the relative amplitude of the DAP as the membrane potential approached E_K (Fig. 4*A*). Nevertheless, slight membrane depolarizations greatly increased the rate of DAP potentiation during repetitive antidromic trains (Fig. 4*B*).

This voltage-dependent increase in dendritic spike broadening and DAP potentiation can not involve Ca^{2+} currents as both dendritic and somatic spikes were insensitive to Cd^{2+} (400 μM) and Ni^{2+} (≤1 mM; n = 12), and focal Cd^{2+} ejections only increased DAP potentiation by blocking a somatic slow AHP (n = 3; data not shown). However, a TTX-sensitive I_{NaP} has been shown to boost synaptic depolarizations in ELL pyramidal cells at both the somatic and dendritic level (Berman et al. 1997, 2001; Turner et al. 1994). Previous studies have shown that low concentrations of phenytoin (30–60 μM) produce a relatively greater block of persistent (I_{NaP}) versus fast inactivating Na^+ currents (Lampl et al. 1998; Segal and Douglas 1997). Focally ejecting phenytoin (75 μM) hyperpolarized the membrane potential in both somatic and dendritic recordings by 5–15 mV with the greatest effects observed in dendritic locations. Phenytoin further decreased dendritic spike amplitude by ≤40% as well as temporal summation of dendritic spikes during antidromic stimulus trains (Fig. 4*C; n* = 6). Similarly, phenytoin ejections at the soma decreased DAP amplitude by ≤50% and substantially decreased DAP potentiation during burst discharge (Fig. 4, *C* and *D; n* = 6).

In a separate set of experiments, we recorded the presence of a slow membrane depolarizing shift in somatic recordings during long current pulses (n = 9/16). The depolarization began within a few 100 ms of current pulse onset and continued at a rate of 2.9 ± 0.83 mV/s (n = 9) to a stable level 4.0 ± 1.8 mV (n = 9) above the initial membrane potential after ~2–3 s (Fig. 4*E*). This slow depolarization was not Ca^{2+} dependent as it was accentuated by focal Cd^{2+} ejections coincident with the reduction of a somatic slow AHP (n = 3). However, we found that this slow depolarizing shift was also rapidly blocked by ejections of phenytoin (Fig. 4*E; n* = 4).

Given that burst discharge was still present after phenytoin application, it is apparent that I_{NaP} is not essential to burst discharge. Rather, I_{NaP} lowers the threshold for burst discharge by boosting the dendritic spike and DAP and promotes a shift from tonic to burst discharge by generating a long depolarizing membrane potential shift. A relatively selective effect by phenytoin on I_{NaP} could be argued based on a general reduction of dendritic spike rate of rise, amplitude, and rate of repolarization (Fig. 4*C*). This result is substantially different from those obtained in response to focal ejections of TTX, which immediately fractionates dendritic spikes into multiple, fast components (Turner et al. 1994). Phenytoin was also able to block substantial portions of both the DAP and slow depolarizing shift without blocking somatic spike discharge. Nevertheless, we could detect a slight (10%) reduction in the amplitude of somatic spikes by the time DAPs were reduced (Fig. 4*C*) that continued with additional phenytoin ejections. These effects on spike discharge are consistent with previous reports that a sufficient concentration of phenytoin also affects fast inactivating Na^+ channels (Lampl et al. 1998; Segal and Douglas 1997). Therefore, to gain a more selective analysis of the role for I_{NaP}, we used a detailed multi-compartmental model of ELL pyramidal cells (see METHODS) (Doiron et al. 2001).

Role for I_{NaP} in modulating somatic and dendritic spike discharge

The ability for a TTX-sensitive I_{NaP} to magnify EPSPs in ELL pyramidal cells has been established experimentally (Berman et al. 1997, 2001) and reproduced in a compartmental model (Doiron et al. 2001). By further examining the role of NaP conductance (g_{NaP}) in this model, we found that g_{NaP} faithfully tracked the time course of both somatic and dendritic spikes (Fig. 5). In the somatic compartment this produced a slight increase in somatic spike amplitude, a depolarization on the falling phase of the spike, and a substantial increase in DAP amplitude (Fig. 5, *A* and *C*). At the dendritic level, I_{NaP} increased both the amplitude and total duration of the dendritic spike (Fig. 5, *B* and *C*). In fact, the effects of I_{NaP} in the

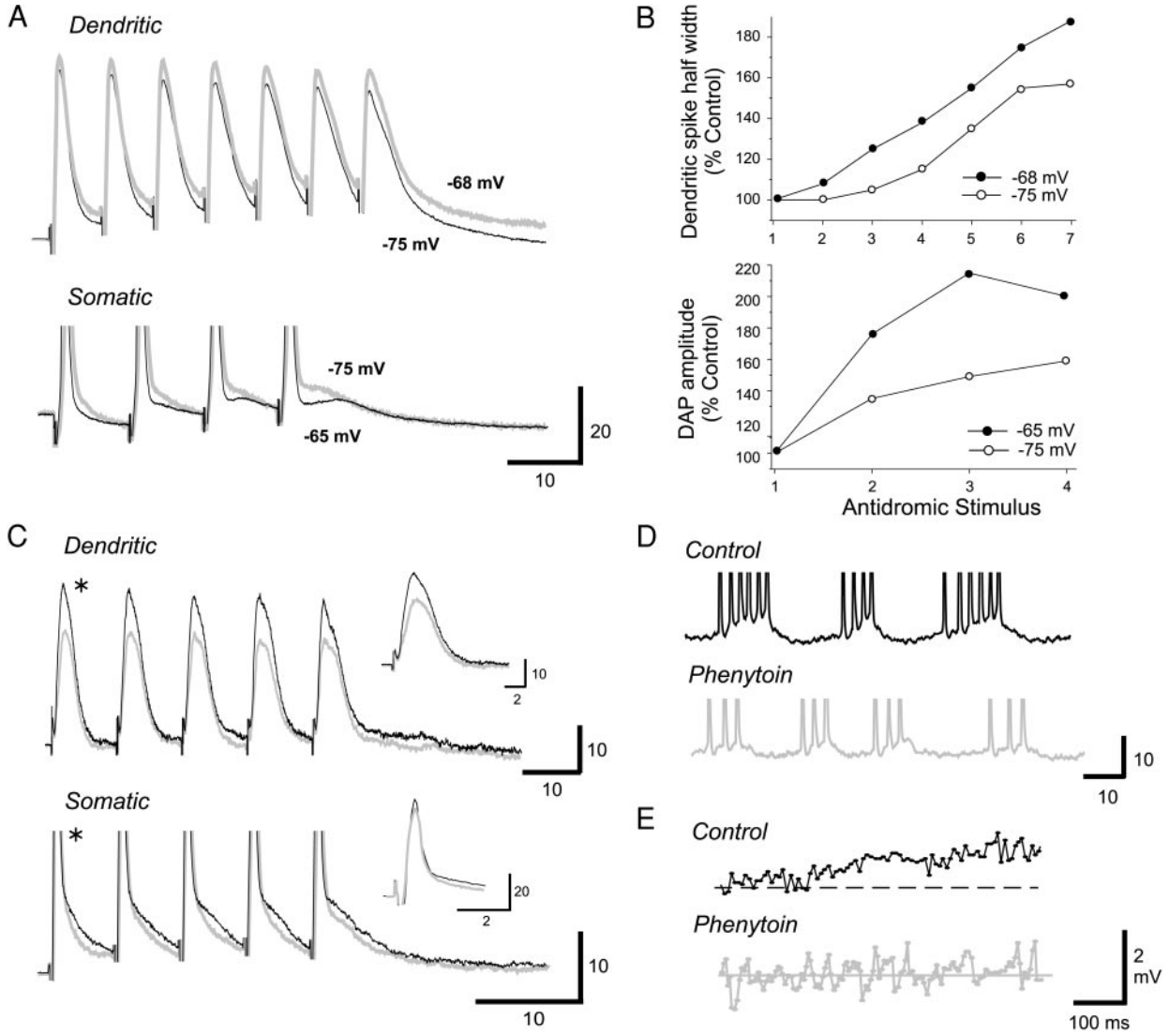

FIG. 4. The rate of dendritic spike broadening and DAP potentiation during a burst are increased by I_{NaP}. *A*: superimposed traces from dendritic and somatic recordings from separate cells in response to antidromic stimulus trains at resting membrane potential (black traces) and during a 7- to 10-mV membrane depolarization (thick gray traces). *B*: plots of the dendritic spike half-width and degree of DAP potentiation for the records shown in *A*. *C*: antidromic stimulus trains recorded in a dendritic and somatic recording indicating a reduction of dendritic spike and DAP amplitude by focal application of 75 μM phenytoin (thick gray traces). *Insets*: expanded views of spikes evoked by the 1st stimulus of the antidromic train (asterisks). *D*: focal application of 75 μM phenytoin (gray trace) reduces the degree of DAP potentiation during burst discharge. *E*: measurement of peak AHP amplitudes during long depolarizing current pulses reveals a slowly rising depolarization that is blocked by 75 μM phenytoin (gray trace). Records in *E* represent an average of 2 traces, and burst AHP amplitudes are omitted for clarity. Somatic spike amplitudes are truncated in *A*, *C*, and *D* for illustrative purposes.

simulations were very similar to those revealed by membrane polarization or phenytoin application (cf. Figs. 4 and 5).

These results are important in indicating that I_{NaP} can boost not only the DAP but also the backpropagating dendritic spike. This characteristic allowed I_{NaP} to magnify the intraburst depolarization at both the somatic and dendritic level. Thus during repetitive discharge at frequencies that led to dendritic spike broadening, g_{NaP} increased the dendritic spike and underlying temporal summation as well as the rate of DAP potentiation (Fig. 6, *A* and *B*).

Previous work established that cumulative inactivation of a dendritic delayed rectifier K^+ current (Dr, d) that led to dendritic spike broadening was a critical variable for inducing conditional backpropagation (Doiron et al. 2001). The addition of I_{NaP} to account for a boost in synaptic potentials lowered the threshold for burst discharge to within the range encountered in pyramidal cells. The primary role of dendritic K^+ current in this process is highlighted by the fact that removing cumulative inactivation of $g_{Dr,d}$ prevented the increase in somatic and dendritic g_{NaP} during a spike burst (Fig. 6, *C* and *D*). The inverse relationship between these currents was also apparent in a simultaneous decrease in $g_{Dr,d}$ (through inactivation) and an increase in the baseline g_{NaP} during dendritic spike summation (Fig. 6, *E* and *F*). These data indicate that the increase in g_{NaP} during a burst depends upon the initial inactivation of dendritic K^+ current. Thus $g_{Dr,d}$ and g_{NaP} act in a synergistic fashion to augment the dendritic spike and rate of DAP potentiation during repetitive discharge.

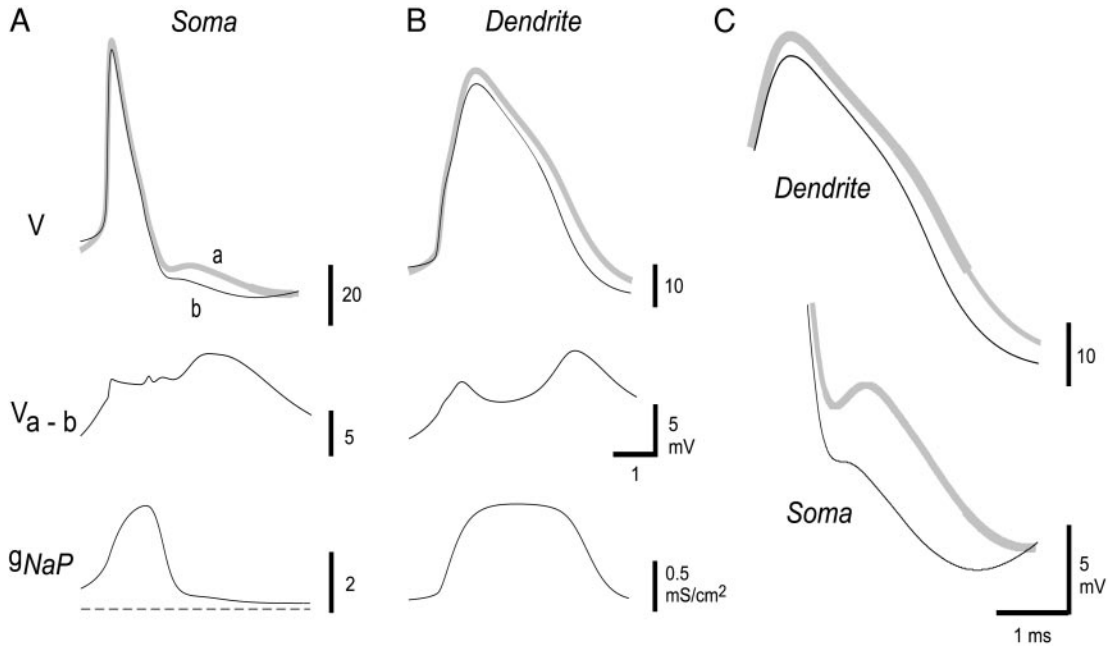

FIG. 5. I_{NaP} augments the somatic DAP and dendritic spike. *A–C*: measurements of membrane voltage and I_{NaP} conductance (g_{NaP}) in the soma (*A*) and proximal dendrites (*B*) of a compartmental model of pyramidal cells. *A* and *B*, *top*: superimposed voltage traces (*V*) shown either with g_{NaP} (gray trace) or without g_{NaP} (black trace). *Middle*: the difference between voltage responses with or without g_{NaP} (V_{a-b}). *Bottom*: plots of g_{NaP} associated with somatic and dendritic responses. Dashed line on bottom left indicates the 0 conductance level. Potentials in *C* are expanded and superimposed views of the dendritic spike and somatic DAP either with g_{NaP} (gray trace) or without g_{NaP} (black trace). Note that g_{NaP} enhances the DAP at the soma and both the peak and duration of the dendritic spike. Although the effects of g_{NaP} in the somatic compartment are truncated by repolarizing K^+ currents (*A*), it is still capable of increasing DAP amplitude. Applied current was adjusted to maintain a constant spike frequency using $I_{applied} = 0.3$ nA in *A* and 0.9 nA in *B* to offset the effects of removing g_{NaP}. To improve spike resolution, the simulation integrative time step was set to 5 μs as compared to 25 μS for all other simulations.

I_{NaP} underlies the transition from tonic to burst discharge and shifts in oscillation period

Burst discharge during short current pulses (100 ms) is dependent on the ISI of spike discharge falling between 3 and 14 ms (Lemon and Turner 2000). A transition to burst discharge during long depolarizations might then occur through a progressive decrease in ISI. In agreement with this, we found that cells exhibiting a prolonged initial period of tonic activity switched to burst discharge once the ISIs fell below ~12 ms ($n = 6$) with all cells discharging bursts at ISIs within 8–16 ms ($n = 16$). After burst onset, the ISIs remained essentially stable throughout the remainder of the depolarization (not considering burst AHP or spike doublet ISIs) with no clear trends over time despite a reliable decrease in oscillation period (Fig. 7*A*). We found that cells exhibiting a clear decrease in ISI leading up to burst discharge also presented a well-defined slow depolarizing shift in membrane potential (Fig. 7*A*). An ISI reduction was most prevalent during the steepest rate of increase in the membrane depolarizing shift. The rate of decrease in ISI then slowed in conjunction with a slower rate of change in the membrane depolarization.

Unlike the results obtained for pyramidal cells, examination of the compartmental model in its original formulation revealed that long-duration current pulses did not invoke a decrease in ISI or a depolarizing membrane potential shift (Fig. 7*B*). Thus depolarizations set initially to evoke tonic discharge did not shift to burst discharge but simply maintained the initial level of tonic activity (data not shown). If the depolarization began at a level above burst threshold, the model failed to produce any further decrease in oscillation period over time (Fig. 7*B*).

To simulate a phenytoin-sensitive slow depolarization, we replaced I_{NaP} with $I_{NaP,S}$ to introduce a second slower time constant for NaP activation that matched the rate of the slow depolarizing shift in pyramidal cells (termed $I_{NaP,S}$, $\tau_s = 1.5$ s; see METHODS). With the addition of this kinetic parameter, depolarizations initially set to generate tonic spike discharge produced a gradual decrease in ISI to ~8 ms prior to the onset of burst discharge (Fig. 7*C*). Spike discharge was further accompanied by a slow depolarizing shift that promoted a shift from tonic to burst discharge (Fig. 7*C*). Once burst discharge was triggered, the oscillation period decreased ~50 ms over time (Fig. 7*C*); a value within the range expected in pyramidal cells (Fig. 7, *A* vs. *C*).

Given the role for I_{NaP} in augmenting the dendritic spike and DAP (Figs. 5 and 6), we examined whether $I_{NaP,S}$ could exert additional affects on spike discharge during long depolarizations (Fig. 8). This analysis determined that the transition from tonic to burst discharge was marked by an increase in dendritic spike duration and DAP amplitude due to the increase in $I_{NaP,S}$ (Fig. 8, *B* and *C*). The continued increase in $I_{NaP,S}$ further affected spike properties during burst discharge by increasing the rate of DAP potentiation from one burst to the next (Fig. 8*D*). The increase in DAP potentiation had the important effect of triggering a somatic spike doublet in a shorter period of time; thereby reducing burst duration and oscillation period (Fig. 8, *B* and *D*; DAP potentiation denoted by dashed lines).

Therefore the addition of $I_{NaP,S}$ allowed the model to suc-

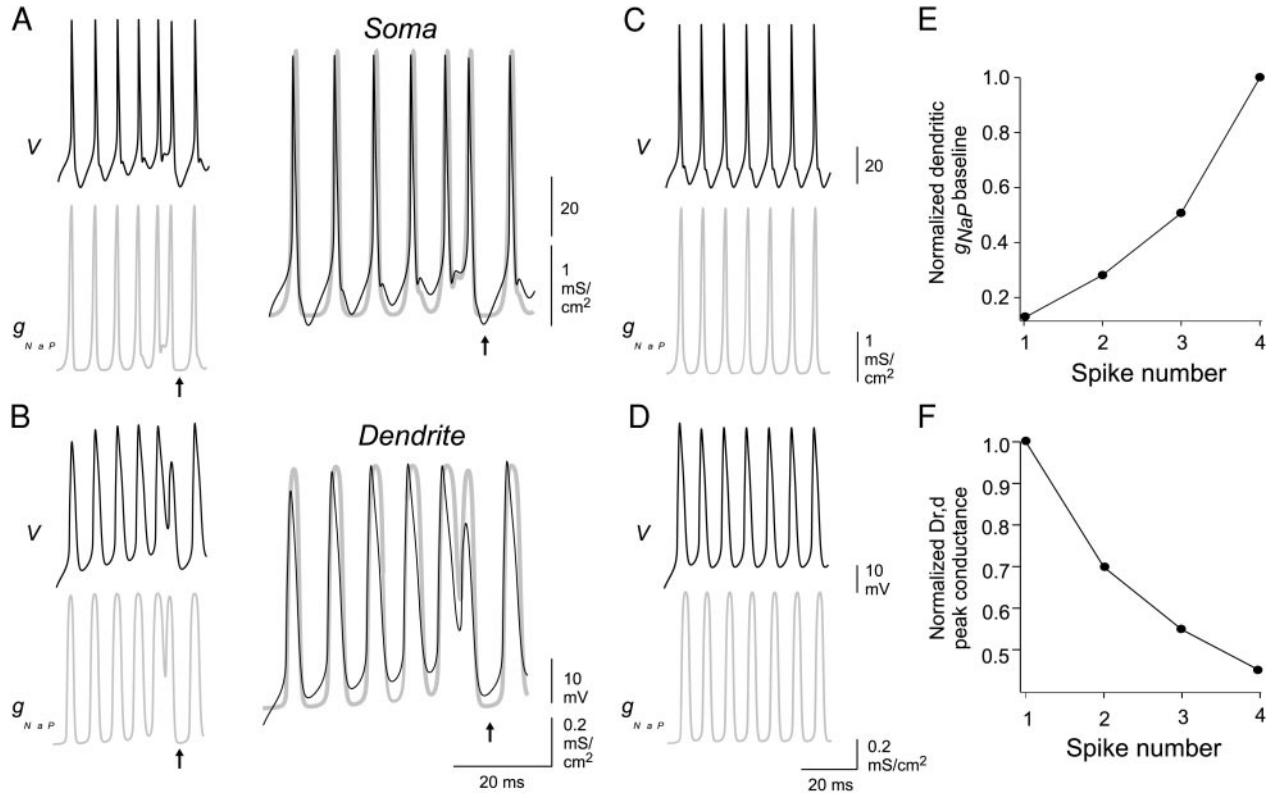

FIG. 6. I_{NaP} augments the DAP and dendritic spikes during burst discharge. *A* and *B*: response of the compartmental model to 0.75 nA applied current with a spike burst (*V*) plotted in conjunction with NaP conductance (g_{NaP}) in the soma (*A*) and proximal dendritic compartments (*B*). g_{NaP} plots are shown in gray and arrows indicate burst AHPs. *Insets* (to the *right* in *A* and *B*): expanded and superimposed plots of *V* and g_{NaP} at the soma and dendrite. Note that g_{NaP} increases through a burst and tracks voltage excursions associated with both the somatic DAP and dendritic spike. *C* and *D*: spike bursts and the associated change in g_{NaP} at the soma (*C*) and dendrite (*D*) are blocked by removing cumulative inactivation of $g_{Dr,d}$ from the model. *E* and *F*: plots of the increase in g_{NaP} at the base of dendritic spikes (*E*) and cumulative inactivation of dendritic K^+ current (*F*; $g_{Dr,d}$) for the bursts shown in *A* and *B*. Plots are normalized to the maximal change from the original baseline in each case.

cessfully reproduce essentially all aspects of spike output in pyramidal cells. This agreement between experimental data and simulations strongly support the hypothesis that the rate of DAP potentiation controls oscillation period by regulating the time required to trigger a spike doublet. The results further indicate a control over conditional backpropagation on two time scales. One is exerted by I_{NaP} within each spike burst as a positive feedback mechanism with respect to the degree of dendritic K^+ current inactivation (Fig. 6). The second occurs when a slow activation of I_{NaP} (modeled as $I_{NaP,S}$) modulates the gain of this interaction on a scale of seconds (Fig. 8).

Application of dynamical systems theory to control of burst output

We recently reduced the large compartmental model used in this study to a two-compartmental version composed of six differential equations (Doiron et al. 2002). The advantage in performing this simplification is that it allowed a detailed dynamical systems treatment of conditional backpropagation for comparison to other burst models (Izhikevich 2000; Rinzel and Ermentrout 1989; for a review of dynamical systems, see Strogatz 1994). The ensuing system, referred to as the Ghostburster, reproduced most aspects of conditional backpropagation and presented key predictions regarding the factors that could regulate oscillation period (Doiron et al. 2002). We now test some qualitative predictions arising from Doiron et al. (2002) to relate specific aspects of the Ghostbursting mechanism to ionic factors that influence the DAP and spike output within a burst.

A convenient method to illustrate the dynamics of our reduced model is to construct ISI return maps (ISI_{i+1} vs ISI_i). Figure 9*A* shows the somatic voltage of the Ghostburster equations during a single burst evoked by an applied current (I_{app}) together with the associated ISI return map, where the diagonal $ISI_{i+1} = ISI_i$ partitions the map into burst and interburst regions. As a single burst evolves, its ISI sequence traces a curve in the return map. The sequence begins at a high value in the burst region, and then shifts along the diagonal as the ISIs within the burst decrease (1). The doublet ISI invokes a sharp descent in the sequence (2), which is followed by an injection of the sequence to a higher value in the interburst region corresponding to the burst AHP duration (3). Finally, the sequence is reinjected back into the burst region and a new burst begins (4).

Viewing the burst trajectory with ISI return maps also illustrates two related dynamical systems concepts: saddle-node bifurcation and trapping region. Bifurcations characterize qualitative changes in system dynamics as a parameter, or set of parameters, is varied (see Strogatz 1994). In particular, saddle-node bifurcations occur when a stable fixed point attractor coalesces with an unstable saddle point. After the bifurcation,

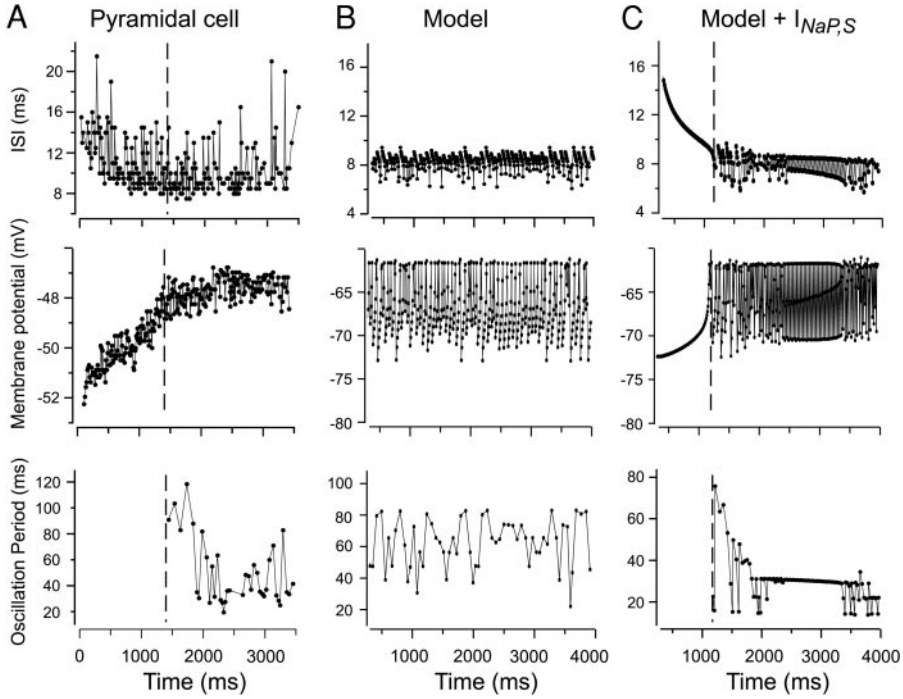

FIG. 7. A slow component of I_{NaP} accounts for the transition from tonic to burst discharge and shifts in oscillation period during prolonged depolarizations. *A*: response of a pyramidal cell somatic recording to a 0.4 nA, 4 s current injection. Cell output begins as tonic spike discharge and then shifts to burst discharge (transition indicated by - - -). During the period of tonic spike discharge the ISI decreases steadily to ~9 ms at the point of burst onset (*top*). Plotting the membrane potential as the peak negative voltage of AHPs (troughs) reveals a steady depolarization through the course of current injection (*middle*), followed by a decrease in oscillation period over time (*bottom*). For illustrative purposes, the values associated with the burst AHP and spike doublets have been excluded, removing the overlying increase in variability of ISI and membrane potential at burst onset (cf. Fig. 2*C*). *B*: plots of the output of the compartmental model containing the initial kinetic parameters of I_{NaP} when activated by a 0.6 nA, 4 s current injection that was set initially above threshold for burst discharge. Note that the model fails to exhibit a shift in ISI (*top*), a membrane depolarizing shift (*middle*), or a change in oscillation period over time (*bottom*). *C*: the slow depolarizing shift observed in pyramidal cells was simulated by incorporating a 2nd time constant for I_{NaP} activation ($I_{NaP,S}$; τ = 1.5 s). This longer $I_{NaP,S}$ permits the model to shift from tonic to burst mode in association with a decrease in ISI (*top*), a slow membrane depolarization (*middle*), and a decrease in oscillation period over time (*bottom*) once bursting is initiated. The segments of regular burst behavior between ~2 and 3 s in *C* arises from a window of periodic behavior bordered by chaotic dynamics, a characteristic property of chaotic systems (Strogatz 1994).

the system's trajectory no longer evolves to the stable fixed point but to a new attractor that is often system dependent. We have shown that a saddle-node bifurcation transitions the Ghostburster equation dynamics from a single fixed point attractor reflecting tonic discharge (a single point on the diagonal line $ISI_{i+1} = ISI_i$) to a chaotic strange attractor that produces the burst curve shown in Fig. 9*A* (Doiron et al. 2002). Dynamical systems near saddle-node bifurcations have a trapping region where trajectories have low velocities through phase space (Strogatz 1994). This translates to a fine control of the time scale of the dynamics by choosing the proximity to the bifurcation in parameter space. The trapping region in the Ghostburster system is reflected by the ISI sequence clustering about the diagonal $ISI_{i+1} = ISI_i$ (region 1 in Fig. 9*A*). The sequence must pass through the trapping region before it can finally escape and produce the somatic doublet (2), terminating the burst. The time required to traverse the trapping region (the sum of all the ISIs within the region) is approximately the duration of the burst. Hence, control of burst duration, and equivalently oscillation period, reduces to determining the factors that control ISI clustering in the trapping region.

We now consider how $I_{NaP,S}$ controls oscillation period over time within the framework of our dynamical systems analysis of burst discharge. Because the time scale of s is much larger than the time scale of both spikes and bursts (τ_s = 1.5 s), we can treat s as a quasistatic parameter with respect to the fast bursting dynamics (Rinzel and Ermentrout 1989). The effect of a slow increase in s is then similar to an increasing applied depolarization I_{app}. Thus through analogy to the Ghostburster system, the transition from tonic to burst discharge over time is due to the system passing through a saddle-node bifurcation of limit cycles as the slow activation of I_{NaP} increases through some critical value $s = s_{SN}$ (in the quasistatic approximation limit). In addition, the amount of time that the ISI sequence spends in a trapping region reduces as s increases away from the critical value of the saddle-node bifurcation at $s = s_{SN}$. This prediction is supported by comparing ISI return maps for burst discharge in the full compartmental model and pyramidal cell recordings (Fig. 9, *B* and *C*). We specifically compare the return maps at the onset of burst discharge (s is near s_{SN}) to bursts at the end of a long depolarization after the variable s has increased (s is far from s_{SN}). At the onset of burst discharge, the clustering of the ISI sequence near the diagonal in the return map is significant and necessarily the oscillation period of a burst is long. At the end of a long depolarization, the ISI points are further away from the diagonal in the return map and there is significantly less clustering of ISI points. Thus the sequence traverses the trapping region in less time, resulting in

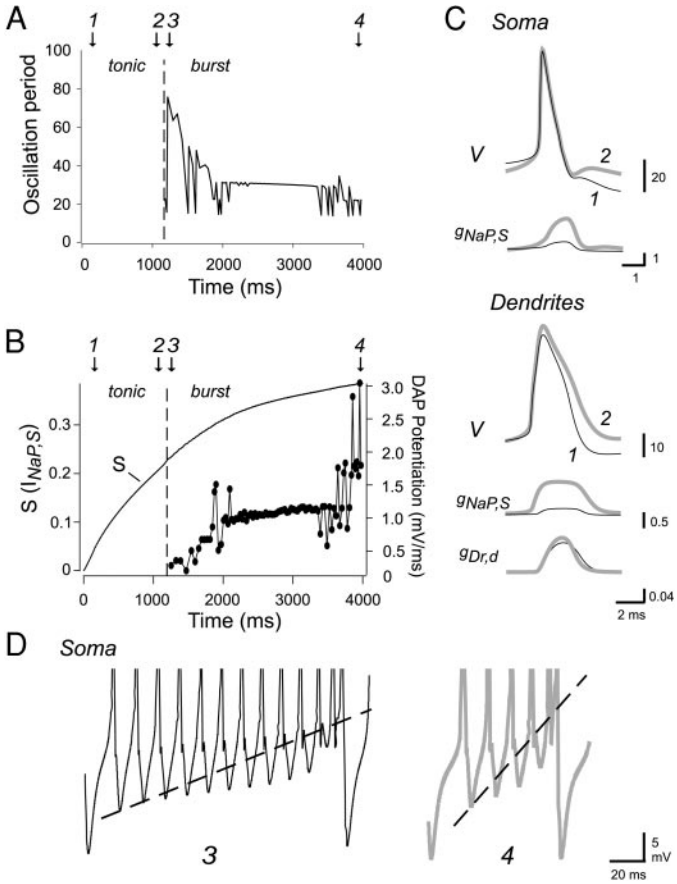

FIG. 8. Oscillation period is controlled over time by the rate of DAP potentiation by $I_{NaP,S}$. *A*: plot of the onset of burst discharge (- - -) and shift in oscillation period over time after 0.6 nA current onset in the compartmental model incorporating $I_{NaP,S}$. *B*: plots of the increase in $I_{NaP,S}$ activation (*s*) and the rate of DAP potentiation over time. Four time points (1–4) are indicated by arrows to compare voltage and current responses shown in *C* and *D*. Note that the rate of DAP potentiation increases over time and changes in concert with oscillation period (compare *A* and *B*). *C*: expanded and superimposed traces of somatic and dendritic spikes (*V*), $g_{NaP,s}$ and $g_{Dr,d}$ at the start of tonic spike discharge (1; black traces) and immediately preceding burst onset at time point 2 (gray traces). Note the increase in DAP amplitude, dendritic spike duration, and $g_{NaP,s}$ by the time of burst onset. *D*: expanded and superimposed traces of somatic spike bursts at time points 3 (black trace) and 4 (gray trace). Dashed lines denote the rate of DAP potentiation during a spike burst (also plotted in *B*). Note that the increased rate of DAP potentiation at time point 4 generates a somatic spike doublet in a shorter period of time, resulting in a shorter burst duration and oscillation period.

shorter oscillation periods compared to those of the earlier bursts.

DISCUSSION

This study identifies the mechanisms by which a principle sensory neuron can initiate burst discharge and provide fine control over oscillation period. Both endpoints are achieved by regulating the *time* required to trigger a spike doublet that periodically blocks spike backpropagation into apical dendrites. Experimental analysis and compartmental modeling identify a key role for I_{NaP} in modulating both the dendritic spike and DAP over two distinct time frames to control spike doublet generation, and thus oscillation period. A dynamical systems analysis reveals that the ionic interactions underlying this process control the rate of transition through a trapping region connected to a saddle-node bifurcation of limit cycles that separates tonic and burst output in pyramidal cells.

Control of oscillation period

The oscillation period for burst discharge is most often determined by the kinetic properties of voltage-dependent ion channels such as I_T or I_h (Destexhe et al. 1998; Dickson et al. 2000; Huguenard 1996), intrinsic membrane resonance (Hutcheon and Yarom 2000), or by the frequency and timing of synaptic inputs in the network (Booth and Bose 2001; Buzsaki and Chrobak 1995). In ELL pyramidal cells, the success of Na^+ spike backpropagation controls cell output by regulating somatic membrane excitability (Doiron et al. 2001; Lemon and Turner 2000; Turner et al. 1994). We have now shown that oscillation period in ELL pyramidal cells depends on the rate of occurrence of somatic spike doublets that block spike backpropagation. Both experimental data and simulations indicate that the time required to generate a spike doublet is directly linked to the rate of DAP potentiation during repetitive discharge, thereby controlling oscillation period over a wide range. By comparison, a prominent burst AHP was entirely stable during shifts of $\leq$40 ms in oscillation period. The stability of the burst AHP proves to be critical, however, in that oscillatory burst discharge would soon fail if the cell did not reset the parameters necessary to induce conditional backpropagation.

The underlying mechanism of burst discharge in pyramidal cells depends on differences between somatic and dendritic spikes to generate a DAP at the soma. A similar process is likely to be found in other cells in which backpropagating spikes produce a somatic DAP (Golding et al. 1999; Larkum et al. 1999; Williams and Stuart 1999; Zhang et al. 1993). In ELL pyramidal cells, a steadily decreasing ISI leads to an abrupt loss of spike backpropagation that removes the DAP, generating an interburst interval. By repeating this process of conditional backpropagation, the output pattern is converted from one of tonic discharge to clusters of spikes (bursts) separated by interburst intervals. This periodic activation and loss of excitatory drive is similar to that which produces burst discharge in thalamic neurons, although in this case, the inactivation of I_T and deactivation of I_h leads to the interburst interval (Huguenard and Prince 1992; McCormick and Pape 1990). Interestingly, Na^+ spikes backpropagate over the initial stem dendrites of thalamocortical relay cells that contain the highest density of I_T channels (Williams and Stuart 2000). Because backpropagating spikes will almost certainly activate I_T channels, burst termination by an inactivation of I_T during a repetitive spike train provides an interesting parallel to the process we have described in ELL pyramidal cells.

Role of persistent Na^+ current

The molecular identity of I_{NaP} has been debated, with evidence that I_{NaP} can arise through the same channels that produce fast inactivating Na^+ current (Alzheimer et al. 1993; Crill 1996; Taddese and Bean 2002). Evidence that other channel subtypes might contribute to persistent Na^+ current(s) come from reports of a larger single-channel conductance for I_{NaP} than fast inactivating Na^+ channels (Magistretti et al. 1999a,b), the ability to achieve a relatively selective block of

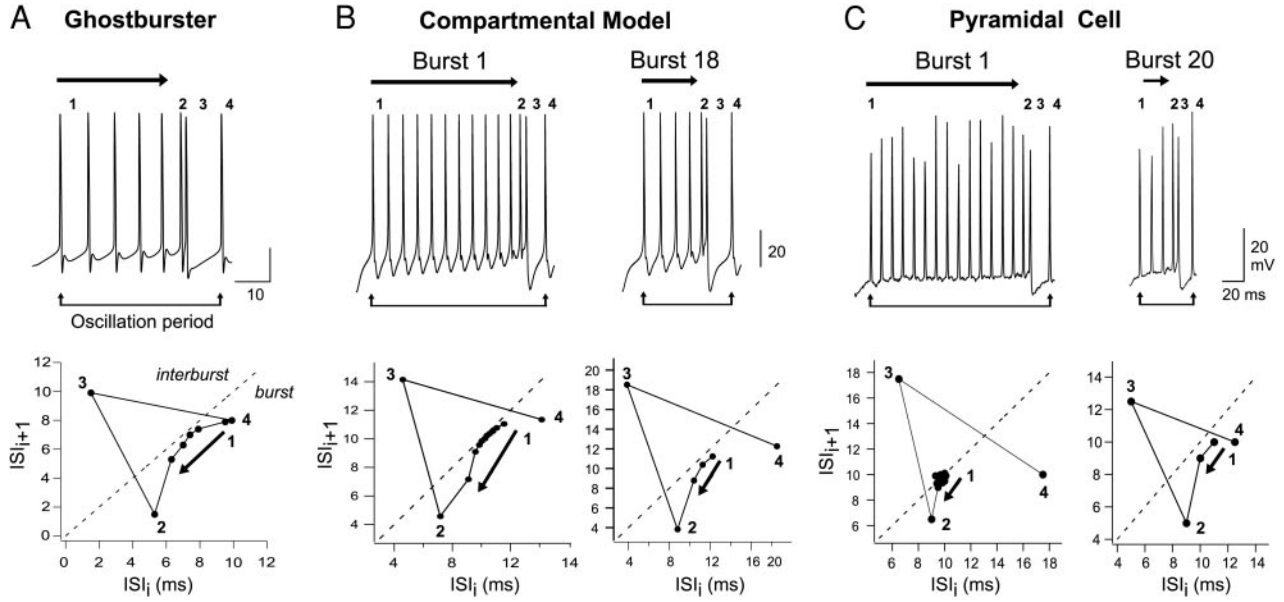

FIG. 9. The interplay between dendritic K^+ current and $I_{NaP,S}$ accounts for the time scale of an intermittent escape from the trapping region of a saddle-node bifurcation. *A–C, top*: single spike bursts from the Ghostburster model incorporating only $g_{Dr,d}$ (*A*), the full compartmental model incorporating $g_{Dr,d}$ and $I_{NaP,S}$ (*B*), and a pyramidal cell recording (*C*). Numbers above spikes correspond to different sections of the burst (see RESULTS). Oscillation period is denoted by linked arrows below each voltage trace. Illustrated for both the compartmental model and pyramidal cell data is the first and later bursts in which oscillation period has decreased during an applied current. *Bottom*: ISI return maps of the spike trains shown in *top*, with the dashed diagonal line corresponding to the expected trajectory for tonic spike discharge ($ISI_{i+1} = ISI_i$). The numbers on the return maps correspond to the sections of the bursts indicated in the traces above. Sections 2–4 are qualitatively the same in all ISI maps. However, section 1 of the early bursts in both model and pyramidal cells (*B* and *C*) shows much more clustering of ISIs than in the later bursts. We note that the transition through the trapping region for the initial long bursts is smooth for the model (*B*) and distorted for the data (*C*). This is to be expected considering the internal noise and finite resolution of the recordings. However, the clustering of ISIs near the diagonal is clear in both model and data.

I_{NaP} pharmacologically (Brumberg et al. 2000; Lampl et al. 1998; Washburn et al. 2000), and the existence of a resurgent Na^+ current in some cell types (Raman and Bean 1997). Our work does not attempt to distinguish between these possibilities. Rather we used low concentrations of phenytoin to obtain a relatively selective block of I_{NaP}. Although results from these experiments strongly implicate I_{NaP} in modulating the DAP, additional effects by phenytoin on somatic spike amplitude encouraged us to focus on compartmental modeling to fully examine its role independently of fast inactivating Na^+ channels. The close match between experimental data and simulations provides convincing evidence that a persistent component of Na^+ conductance augments somatic and dendritic factors underlying burst discharge.

I_{NaP} has been shown to contribute to a wide range of membrane depolarizations, including subthreshold synaptic potentials and oscillations, low-threshold Ca^{2+} spikes, DAPs, and somatic spike bursts (Agrawal et al. 2001; Alonso and Llinas 1989; Azouz et al. 1996; Berman et al. 2001; Brumberg et al. 2000; Mantegazza et al. 1998; Parri and Crunelli 1998; Stuart and Sakmann 1995; Wang 1999; Washburn et al. 2000). I_{NaP} channel activity has also been directly recorded in dendritic regions (Magee and Johnston 1995a,b; Magistretti et al. 1999a; Stuart and Sakmann 1995). However, to our knowledge, the only other work to assess the role for dendritic I_{NaP} in modulating burst discharge was a theoretical study (Wang 1999). We have now shown that I_{NaP} acts to enhance backpropagating dendritic Na^+ spikes and the depolarization arising from temporal summation of dendritic spikes during repetitive discharge. The effects of I_{NaP} were linked to the initial cumulative inactivation of dendritic K^+ current within a burst and an additional long time constant for activation ($I_{NaP,S}$). The influence of persistent Na^+ current can thus be segregated into an intraburst mechanism that permits I_{NaP} to magnify the key elements underlying conditional backpropagation and a longer activation time ($I_{NaP,S}$) that modulates the gain of the intraburst mechanism to control burst frequency over time.

I_{NaP} most often shows little or no inactivation over the time frame studied here (Crill 1996). However, there are reports that I_{NaP} in some cells can begin to inactivate during long step commands under voltage clamp (~40% inactivation for a 4-s step command to −40 mV) (Magistretti and Alonso 1999). We are uncertain as to whether this occurs in ELL pyramidal cells. However, if it does, it is apparently not sufficient to prevent the continued activation and growth of a significant phenytoin-sensitive slow depolarizing shift (Fig. 4*E*). We are unaware of any reports of an additional long time constant for activation of I_{NaP}. We have implemented it here as a means to account for the slow depolarizing shift over time. The biophysical basis for such a process will be important to examine, but is beyond the scope of the present study.

Experimental and model characteristics fit dynamical systems theory

Dynamical systems analysis of a simple two-compartmental model of pyramidal cells predicted that a transition from tonic

firing to chaotic bursting is mediated by a saddle-node bifurcation (Doiron et al. 2002). This result prompted a further prediction that the oscillation period of burst discharge could be modulated through fine control of a trapping region born from the bifurcation. The use of ISI return maps establishes that the qualitative predictions arising from the Ghostburster equations are verified in both the full compartmental model and experimental recordings. Although bifurcations separating tonic and burst discharge and the control of burst frequency have been observed in abstract mathematical models of bursting neurons (Terman 1992; Wang 1993), the present work identifies the ionic mechanisms that underlie these events in a real bursting neuron. The ubiquitous nature of saddle-node bifurcations throughout dynamical systems theory (Strogatz 1994) suggests that the mechanism of burst control delineated here may be applicable to a variety of bursting neurons.

We have several further predictions about this form of burst discharge, namely a scaling law for the oscillation period and that the burst dynamics are chaotic (Doiron et al. 2002). The time that a trajectory spends within a trapping region can be shown theoretically to scale as $1/\sqrt{\varepsilon}$, where ε is the distance from the bifurcation within parameter space (Pomeau and Manneville 1980; Strogatz 1994). A direct experimental verification of this scaling in ELL pyramidal cell data is problematic. A scaling law has been shown to be dependent upon underlying stochastic processes (Kye and Kim 2000) which are difficult to assess from experimental recordings. Furthermore, the experimental bifurcation parameter is predicted to be the slow NaP activation *s*, which cannot be measured or controlled in a graded manner within experiments. We were thus satisfied that the qualitative nature of the $1/\sqrt{\varepsilon}$ scaling law is observed in both the large model and the experimental recordings, i.e. the monotonic decrease of ISI clustering as *s* increases past s_{SN}. In addition, our theoretical analysis of this burst mechanism predicted a chaotic spike discharge (Doiron et al. 2002). Distinguishing whether deterministic chaos or stochastic processes underlie unpredictability within time series data gained from experiments is often a difficult problem (Eckmann and Ruelle 1992; Theiler et al. 1992). The small number of spike events in each recording (~400) coupled with the nonstationarity of the data sets introduced by the slow activation of NaP makes a clear verification of whether this form of burst discharge is intrinsically chaotic quite challenging and was thus not addressed in this study.

Burst discharge in electrosensory processing

Spike bursts are recorded in ELL pyramidal cells in vivo and have been shown to detect specific features of sensory input (Gabbiani et al. 1996; Metzner et al. 1998). Depolarizations of the duration used here are expected to be encountered in vivo in response to gradual shifts in electric field strength (Bastian 1999; Bastian and Nguyenkim 2001; Bastian et al. 2002). In fact, global electrical field stimuli simulating electrocommunicative interactions between conspecifics was recently shown to induce burst discharge in vivo through a process of conditional backpropagation (J. Bastian, personal communication). The ability for descending synaptic feedback to activate I_{NaP} in pyramidal cells (Berman et al. 1997, 2001) allows one to predict that synaptic activity will be capable of modifying conditional backpropagation and burst discharge. Should synaptic inputs promote a transition between tonic and burst discharge, it could further induce a switch between stimulus estimation and detection during sensory processing. In this regard, it now appears that pyramidal cells can shift their coding strategy from estimation to detection depending on the spatial distribution of input over pyramidal cell receptive fields (Bastian et al. 2002; Gabbiani et al. 1996). However, the encoding capabilities of pyramidal cells will almost certainly be influenced by the intrinsic (cellular) dynamics exposed in the current study. The details of how conditional backpropagation and network dynamics interact and their summed effects upon spike patterning and stimulus encoding remain to be determined.

We acknowledge the support of Drs. A. Longtin and L. Maler of the University of Ottawa as B. Doiron's graduate program supervisors. Critical reading of the manuscript by C. Laing, J. Lewis, and L. Maler is greatly appreciated.

This work was supported by a Canadian Institute of Health Research Grant and Alberta Heritage Foundation for Medical Research (AHFMR) senior scholarship to R. W. Turner. L. Noonan was supported by an AHFMR studentship, L. Noonan and B. Doiron by National Science and Engineering Research Council postgraduate fellowships, and N. Lemon by a Medical Research Council studentship.

REFERENCES

Agrawal N, Hamam BN, Magistretti J, Alonso A, and Ragsdale DS. Persistent sodium channel activity mediates subthreshold membrane potential oscillations and low-threshold spikes in rat entorhinal cortex layer V neurons. *Neuroscience* 102: 53–64, 2001.

Alonso A and Llinas RR. Subthreshold Na+-dependent theta-like rhythmicity in stellate cells of entorhinal cortex layer II. *Nature* 342: 175–177, 1989.

Alzheimer C, Schwindt PC, and Crill WE. Modal gating of Na+ channels as a mechanism of persistent Na+ current in pyramidal neurons from rat and cat sensorimotor cortex. *J Neurosci* 13: 660–673, 1993.

Azouz R, Jensen MS, and Yaari Y. Ionic basis of spike after-depolarization and burst generation in adult rat hippocampal CA1 pyramidal cells. *J Physiol (Lond)* 492: 211–223, 1996.

Bastian J. Plasticity of feedback inputs in the apteronotid electrosensory system. *J Exp Biol* 202: 1327–1337, 1999.

Bastian J, Chacron M, and Maler L. Receptive field organization determines pyramidal cell stimulus encoding capability and spatial stimulus selectivity. *J Neurosci* 22: 4577–4590, 2002.

Bastian J and Nguyenkim J. Dendritic modulation of burst-like firing in sensory neurons. *J Neurophysiol* 85: 10–22, 2001.

Berman N, Dunn RJ, and Maler L. Function of NMDA receptors and persistent sodium channels in a feedback pathway of the electrosensory system. *J Neurophysiol* 86: 1612–1621, 2001.

Berman NJ, Plant J, Turner RW, and Maler L. Excitatory amino acid receptors at a feedback pathway in the electrosensory system: implications for the searchlight hypothesis. *J Neurophysiol* 78: 1869–1881, 1997.

Booth V and Bose A. Neural mechanisms for generating rate and temporal codes in model CA3 pyramidal cells. *J Neurophysiol* 85: 2432–2445, 2001.

Brumberg JC, Nowak LG, and McCormick DA. Ionic mechanisms underlying repetitive high-frequency burst firing in supragranular cortical neurons. *J Neurosci* 20: 4829–4843, 2000.

Buzsaki G and Chrobak JJ. Temporal structure in spatially organized neuronal ensembles: a role for interneuronal networks. *Curr Opin Neurobiol* 5: 504–510, 1995.

Crill W. Persistent sodium current in mammalian central neurons. *Annu Rev Physiol* 58: 349–362, 1996.

Destexhe A, Neubig M, Ulrich D, and Huguenard J. Dendritic low-threshold calcium currents in thalamic relay cells. *J Neurosci* 18: 3574–3588, 1998.

Dickson CT, Magistretti J, Shalinsky MH, Fransen E, Hasselmo ME, and Alonso A. Properties and role of *I*(h) in the pacing of subthreshold oscillations in entorhinal cortex layer II neurons. *J Neurophysiol* 83: 2562–2579, 2000.

Doiron B, Laing C, Longtin A, and Maler L. Ghostbursting: a novel neuronal burst mechanism. *J Comput Neurosci* 12: 5–25, 2002.

Doiron B, Longtin A, Turner RW, and Maler L. Model of gamma frequency burst discharge generated by conditional backpropagation. *J Neurophysiol* 86: 1523–1545, 2001.

Eckmann JP and Ruelle D. Fundamental limitations for estimating dimensions and lyaponov exponents in dynamic systems. *Phys D* 56: 185–187, 1992.

Gabbiani F and Koch C. Principles of spike train analysis. In: *Methods in Neuronal Modeling: From Ions to Networks,* edited by Segev I. Cambridge, MA: MIT Press, 1998, p. 313–360.

Gabbiani F, Metzner W, Wessel R, and Koch C. From stimulus encoding to feature extraction in weakly electric fish. *Nature* 384: 564–567, 1996.

Golding NL, Jung HY, Mickus T, and Spruston N. Dendritic calcium spike initiation and repolarization are controlled by distinct potassium channel subtypes in CA1 pyramidal neurons. *J Neurosci* 19: 8789–8798, 1999.

Gray CM and McCormick DA. Chattering cells: superficial pyramidal neurons contributing to the generation of synchronous oscillations in the visual cortex. *Science* 274: 109–113, 1996.

Hines M and Carnevale N. The neuron simulation environment. *Neural Comp* 9: 1179–1209, 1997.

Holt GR, Softky WR, Koch C, and Douglas RJ. Comparison of discharge variability in vitro and in vivo in cat visual cortex neurons. *J Neurophysiol* 75: 1806–1814, 1996.

Huguenard JR. Low-threshold calcium currents in central nervous system neurons. *Annu Rev Physiol* 58: 329–348, 1996.

Huguenard JR and Prince DA. A novel T-type current underlies prolonged Ca(2+)-dependent burst firing in GABAergic neurons of rat thalamic reticular nucleus. *J Neurosci* 12: 3804–3817, 1992.

Hutcheon B and Yarom Y. Resonance, oscillation and the intrinsic frequency preferences of neurons. *Trends Neurosci* 23: 216–222, 2000.

Izhikevich EM. Neural excitability, spiking, and bursting. *Int J Bifurc Chaos* 10: 1171–1269, 2000.

Kye WH and Kim CH. Characteristic relations of type-I intermittency in the presence of noise. *Phys Rev E* 62: 6304–6307, 2000.

Lampl I, Schwindt P, and Crill W. Reduction of cortical pyramidal neuron excitability by the action of phenytoin on persistent Na+ current. *J Pharmacol Exp Ther* 284: 228–237, 1998.

Larkum ME, Kaiser KM, and Sakmann B. Calcium electrogenesis in distal apical dendrites of layer 5 pyramidal cells at a critical frequency of back-propagating action potentials. *Proc Natl Acad Sci USA* 96: 14600–14604, 1999.

Lemon N and Turner RW. Conditional spike backpropagation generates burst discharge in a sensory neuron. *J Neurophysiol* 89: 1519–1530, 2000.

Lisman JE. Bursts as a unit of neural information: making unreliable synapses reliable. *Trends Neurosci* 20: 38–43, 1997.

Magee JC and Johnston D. Characterization of single voltage-gated Na^+ and Ca^{2+} channels in apical dendrites of rat CA1 pyramidal neurons. *J Physiol (Lond)* 487: 67–90, 1995a.

Magee JC and Johnston D. Synaptic activation of voltage-gated channels in the dendrites of hippocampal pyramidal neurons. *Science* 268: 301–304, 1995b.

Magistretti J and Alonso A. Biophysical properties and slow voltage-dependent inactivation of a sustained sodium current in entorhinal cortex layer-II principal neurons: a whole-cell and single-channel study. *J Gen Physiol* 114: 491–509, 1999.

Magistretti J, Ragsdale DS, and Alonso A. Direct demonstration of persistent Na+ channel activity in dendritic processes of mammalian cortical neurons. *J Physiol (Lond)* 521: 629–636, 1999a.

Magistretti J, Ragsdale DS, and Alonso A. High conductance sustained single-channel activity responsible for the low-threshold persistent Na(+) current in entorhinal cortex neurons. *J Neurosci* 19: 7334–7341, 1999b.

Mantegazza M, Franceschetti S, and Avanzini G. Anemone toxin (ATX II)-induced increase in persistent sodium current: effects on the firing properties of rat neocortical pyramidal neurons. *J Physiol (Lond)* 507: 105–116, 1998.

McCormick DA and Pape HC. Properties of a hyperpolarization-activated cation current and its role in rhythmic oscillation in thalamic relay neurons. *J Physiol (Lond)* 431: 291–318, 1990.

Metzner W, Koch C, Wessel R, and Gabbiani F. Feature extraction by burst-like spike patterns in multiple sensory maps. *J Neurosci* 18: 2283–2300, 1998.

Pape HC. Queer current and pacemaker: the hyperpolarization-activated cation current in neurons. *Annu Rev Physiol* 58: 299–327, 1996.

Parri HR and Crunelli V. Sodium current in rat and cat thalamocortical neurons: role of a non-inactivating component in tonic and burst firing. *J Neurosci* 18: 854–867, 1998.

Pomeau Y and Manneville P. Intermittent transition to turbulence in dissipative dynamical systems. *Comm Math Phys* 74: 189–197, 1980.

Raman IM and Bean BP. Resurgent sodium current and action potential formation in dissociated cerebellar Purkinje neurons. *J Neurosci* 17: 4517–4526, 1997.

Rinzel J and Ermentrout GB. Analysis of neural excitability and oscillations. In: *Methods in Neuronal Modeling,* edited by Koch G and Segev I. Cambridge, MA: MIT Press, 1989, p. 135–169.

Segal MM and Douglas AF. Late sodium channel openings underlying epileptiform activity are preferentially diminished by the anticonvulsant phenytoin. *J Neurophysiol* 77: 3021–3034, 1997.

Sherman SM. Tonic and burst firing: dual modes of thalamocortical relay. *Trends Neurosci* 24: 122–126, 2001.

Steriade M, Curro Dossi R, and Contreras D. Electrophysiological properties of intralaminar thalamocortical cells discharging rhythmic (approximately 40 Hz) spike-bursts at approximately 1000 Hz during waking and rapid eye movement sleep. *Neuroscience* 56: 1–9, 1993.

Steriade M, Jones EG, and Llinas RR. *Thalamic Oscillation and Signalling.* New York: Wiley & Sons, 1990.

Steriade M, Timofeev I, Durmuller N, and Grenier F. Dynamic properties of corticothalamic neurons and local cortical interneurons generating fast rhythmic (30–40 Hz) spike bursts. *J Neurophysiol* 79: 483–490, 1998.

Strogatz SH. *Nonlinear Dynamics and Chaos with Applications to Physics, Biology, Chemistry, and Engineering.* Reading, MA: Addison-Wesley, 1994.

Stuart G and Sakmann B. Amplification of EPSPs by axosomatic sodium channels in neocortical pyramidal neurons. *Neuron* 15: 1065–1076, 1995.

Taddese A and Bean BP. Subthreshold sodium current from rapidly inactivating sodium channels drives spontaneous firing of tuberomammillary neurons. *Neuron* 33: 587–600, 2002.

Tegner J, Lansner A, and Grillner S. Modulation of burst frequency by calcium-dependent potassium channels in the lamprey locomotor system: dependence of the activity level. *J Comput Neurosci* 5: 121–140, 1998.

Terman D. The transition from bursting to continuous spiking in excitable membrane models. *J Nonlinear Sci* 2: 135–182, 1992.

Theiler J, Eubank S, Longtin A, Galdrikian B, and Farmer JD. Testing for nonlinearity in time series—the method of surrogate data. *Phys D* 58: 77–94, 1992.

Turner RW, Maler L, Deerinck T, Levinson SR, and Ellisman MH. TTX-sensitive dendritic sodium channels underlie oscillatory discharge in a vertebrate sensory neuron. *J Neurosci* 14: 6453–6471, 1994.

Turner RW, Plant JR, and Maler L. Oscillatory and burst discharge across electrosensory topographic maps. *J Neurophysiol* 76: 2364–2382, 1996.

Wang X-J. Genesis of bursting oscillations in the Hindmarsh-Rose model and homoclinicity to a chaotic saddle. *Phys D* 62: 263–274, 1993.

Wang XJ. Fast burst firing and short-term synaptic plasticity: a model of neocortical chattering neurons. *Neuroscience* 89: 347–362, 1999.

Washburn DL, Anderson JW, and Ferguson AV. A subthreshold persistent sodium current mediates bursting in rat subfornical organ neurons. *J Physiol (Lond)* 529: 359–371, 2000.

Williams SR and Stuart GJ. Mechanisms and consequences of action potential burst firing in rat neocortical pyramidal neurons. *J Physiol (Lond)* 521: 467–482, 1999.

Williams SR and Stuart GJ. Action potential backpropagation and somatodendritic distribution of ion channels in thalamocortical neurons. *J Neurosci* 20: 1307–1317, 2000.

Zhang L, Valiante TA, and Carlen PL. Contribution of the low-threshold T-type calcium current in generating the post-spike depolarizing afterpotential in dentate granule neurons of immature rats. *J Neurophysiol* 70: 223–231, 1993.